Modelling and validation of residual stresses induced by heat treatment of AA 7075-T6 samples towards the prediction of part distortion in machining

Mohamed Ali Louhichi[1] • Gerard Poulachon[1] • Philippe Lorong[2] • José Outeiro[1] • Eric Monteiro[2] • Dominique Cotton[1]

[1] Arts et Metiers Institute of Technology, LABOMAP, Université Bourgogne Franche-Comté, HESAM Université, F-71250 Cluny, France

[2] Laboratoire PIMM, Arts et Metiers Institute of Technology, CNRS, Cnam, HESAM Université, 151 Boulevard de l'Hopital, 75013 Paris, France

Corresponding author. Email: mohamedali.louhichi@ensam.eu. Phone: +33 6 25 45 71 06

Abstract

The aim of this paper is the validation of a numerical model dedicated to the determination of the residual stresses distribution induced by the heat treatment of AA 7075-T6 alloy. Particularly an inverse method coupled with optimization algorithms was developed and applied for determining the heat convection coefficients during quenching and tempering. Layer removal method was used to verify experimentally the distribution of residual stresses. This method was modeled and simulated using a developed Finite Element Model (FEM). As the final goal is to predict part distortion during machining and after unclamping, the previous simulation is a first step of modeling material removal. In addition, the contour method was used to evaluate the effects of the temperature gradient on the distribution of residual stresses. The comparison between the experimental and numerical results revealed that this approach could predict the residual stresses distribution induced by heat treatment. The results also prove that the prediction of the midline curvature distortion is possible.

Keywords Residual stresses, Part distortion, Heat treatment, Numerical simulation, AA 7075-T6.

1. Introduction

Aluminum parts are widely used in many industrial sectors such as automotive, medical and aerospace. Despite the massive use of this material, the reduction of part distortions is still a big challenge for productive companies. In fact, the probability of not respecting tolerances due to these distortions is 47%, such rework costs manufacturers up to 10 million USD annually [1]. For example, the wasted materials and corrections related to distortions of the machined parts costs over 290 Billion USD, based on a conducted study of Boeing Company regarding the information on manufacturing of four different aeroplanes [2]. These distortions are due to the redistribution of the residual stresses induced by material removal [3]. Improving residual stresses comprehension permits the control of their distributions in the parts and reduce distortions. According to Koç et al. [4], the main factor of the residual stresses is the quenching during the heat treatment. The immersion of the warmed parts in the quenching fluid generates a thermal gradient between the surface and the center of the parts, which conducts to compressive and tensile residual stresses at the surface and the center of the parts respectively [5].

Many numerical methods can be applied to simulate the residual stresses distribution. Cerutti and Mocellin [3] used a polynomial function to represent the residual stresses distribution in the simulated part. Although this method is based on experimental results residual stresses results, it cannot represent the non-uniform distribution of the residual stresses due to the thermal gradient effects. Jeanmart and Bouvaist [6] developed Ramberg-Osgood model to simulate the quenching of AA 7075. Using this model, the thermomechanical problem is assumed to be uncoupled, i.e. the thermal and mechanical calculations are computed consecutively. This approach can control the complex phenomena involved during the heat treatment process, which leads to a better representation of the residual stresses distribution.

The simulated residual stresses distribution can be validated using several experimental techniques that can be classified into two groups: (1) the non-destructive methods such as X-Ray diffraction [7–10], neutron diffraction [11, 12] and (2) the destructive methods such as the contour method [13–17], the layer removal method [18, 19] and the hole-drilling method [21–23]. The selection of the measurement technique depends on many factors such as the geometry of the part, the number of components of the residual stress tensor to be measured, the cost and availability of the measurement techniques [23]. In this work, a set of raw parts was used to carry out the destructive tests. Moreover, the only interest is the global deformations of the part. So, the first two destructive methods were performed.

Hospers and Vogelesang [18] proposed the layer removal method in 1975. This method can be performed using inexpensive equipment setup and is relatively easy compared to other methods. According to Richer-Trummer et al. [19], the layer can be removed using high speed machining (HSM) due to the low influence on the distortion. This is due to the low effects of the high rotational speed and feed which leads to low forces applied to the material [24]. According to Yang et al. [25] and Cerutti et al. [26], the main cause of the distortion is the residual stresses generated by the manufacturing processes before machining.

The contour method can also be used to measure the residual stresses, which was first introduced by Prime [14]. It is a powerful technique for mapping residual stresses in engineering structures. This method is based on superposition principle introduced by Bueckner [27]. Using the contour method, a two-dimensional (2D) map of the residual stresses acting in a direction normal to the plane of interest can be investigated. Recently, a practice guidance has been published by Hosseinzadeh et al. [15] to explain the different steps of this method. Roy et al. [13] developed a Python package, which is an open-source computational framework for residual stress analysis employing the contour method.

In this paper, an approach for predicting the residual stresses induced by heat treatment of 7075-T6 aluminum alloy plates is proposed. After a rapid presentation of the proposed procedure in section 2, a model of the heat treatment of AA 7075-T6 alloy is developed assuming the thermo-elastoplastic behavior of this material (section 3). Based on the inverse method for determining the heat convection coefficients, the heat treatment model is able to predict the non-uniform distribution of the residual stresses. Section 4 deals with the validation of the simulated residual stresses distribution by using two experimental techniques: layer removal and contour methods. A machining model was also developed considering the residual stresses and the effect of machining sequence [28-29]. Before concluding the paper, a discussion on the obtained results is proposed in section 5.

2. Proposed approach

AA 7075-T6, which is an aluminum alloy where zinc is the main alloying element, is used. This alloy is widely employed in aircraft structural parts due to its excellent mechanical properties such as the good ductility, weight, high strength, toughness, and good resistance to fatigue. Its chemical composition is shown in **Table 1**.

Table 1 *Chemical **c**omposition of 7075-T6 Al alloy*

Element	Al	Zn	Mg	Cu	Fe	Si	Mn	Cr	Ti
W_t%	Base	5,1-6,1	2,1-2,9	1,2-2,0	0,5	0,4	0,3	0,18-0,28	0,2

The several steps of this approach are shown in **Fig.1**. The aluminum plates were heat-treated to eliminate the previous residual stresses and to generate a new distribution. During the heat treatment, instrumented plates with thermocouples were used to determinate the heat exchange coefficients (section 3). The layer removal method was employed to validate the residual stresses distribution (section 4.1). This method was modeled and simulated using FEM and the results were compared to experimental ones (section4.2). In the other hand, the induced residual stresses from the heat treatment were measured using the contour method (section 4.3) and the results were compared to the simulation (section 5).

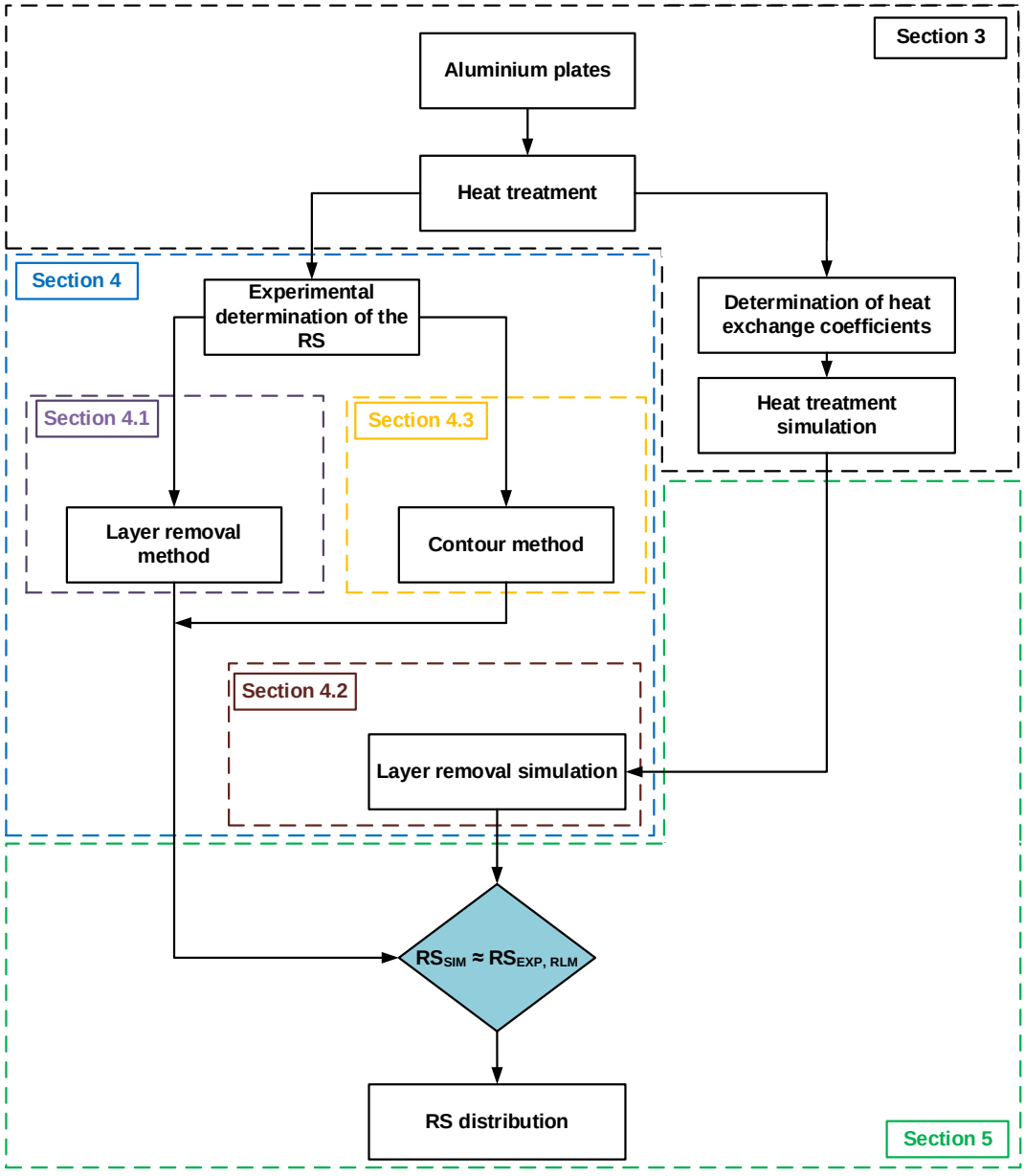

Fig.1 *Flowchart of the proposed approach for determining the RS.*

3. Heat treatment modeling

3.1. Heat treatment process

Quenching and tempering (T6 heat treatment) were applied over samples of 200 mm x 99 mm x 40 mm using the protocol illustrated in **Fig.2** [30]. For quenching, the parts were maintained 470 ° C for 3 hours. This phase before quenching, eliminates the previous residual stresses [6]. During the sudden immersion in the water at 18 °C, an automatic water agitation system was used in order to avoid the calefaction phenomenon. For tempering, the parts were kept at 137 °C for 12 hours and then cooled in the air.

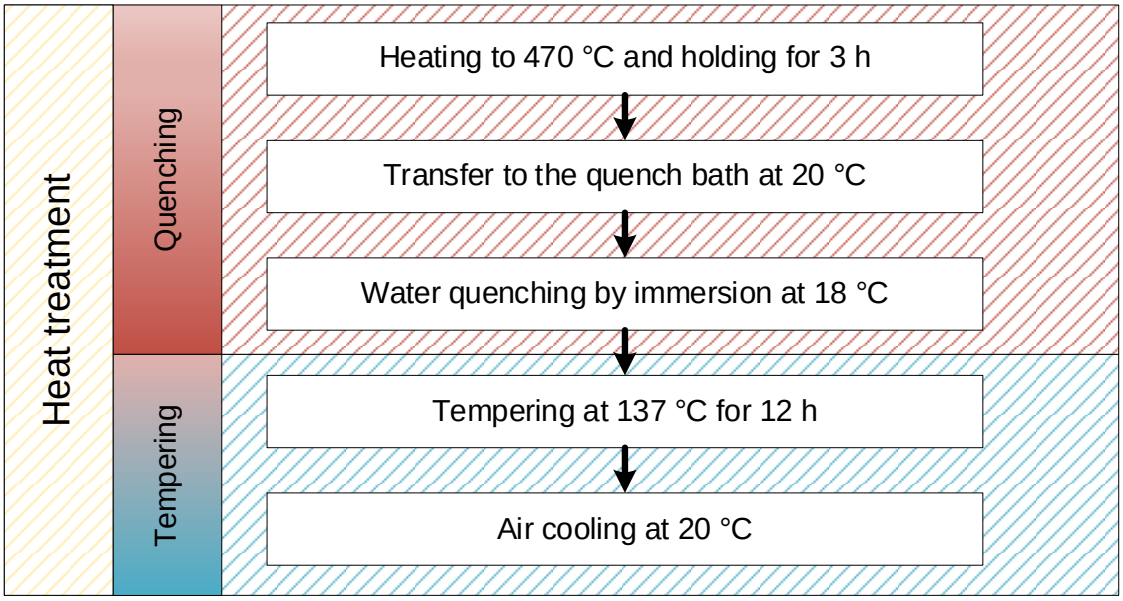

Fig.2 *Protocol of the heat treatment process*

3.2. Experimental determination of heat exchange coefficients

During the heat treatment, a plate was instrumented with thermocouples to measure the variation of temperature during heat treatments. The sample is a rectangular parallelepiped of 200 x 99 x 40 mm. Five holes with 1.2 mm diameter located at 1.6 mm below the surface and in the center of the part were drilled by Electrical Discharge Machining (EDM) in different locations in the plate as shown in **Fig.3**. K-type thermocouples were located at the bottom of each hole. While holding the part in the furnace, all the thermocouples have reached the set temperatures (470 °C during quenching and 137 °C during tempering). The effect of sheath thickness and thermocouple response time were neglected.

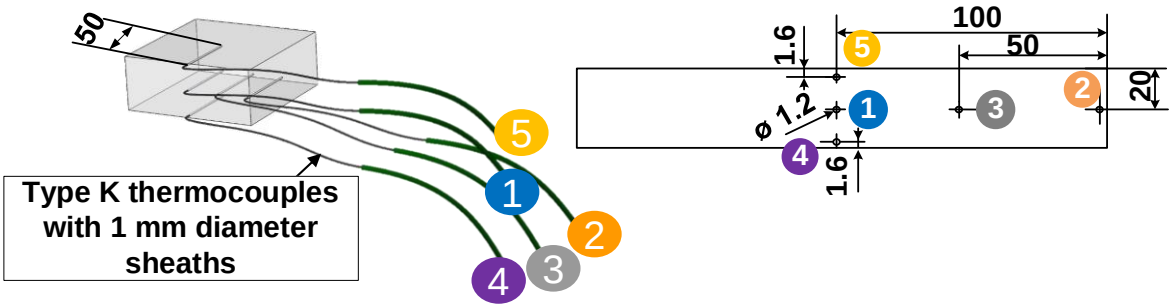

Fig.3 *Location of thermocouples in the AA 7075-T6 plate*

After obtaining the temperature variation as a function of the time from the experiments, numerical simulations under the same experimental conditions were performed using FORGE© software. Using genetic algorithm, the thermal convection coefficients were determined by

minimizing a mean square error cost function. The used genetic algorithm launches iteratively numerical simulations in order to optimize these coefficients. The optimization process is shown in **Fig.4**.

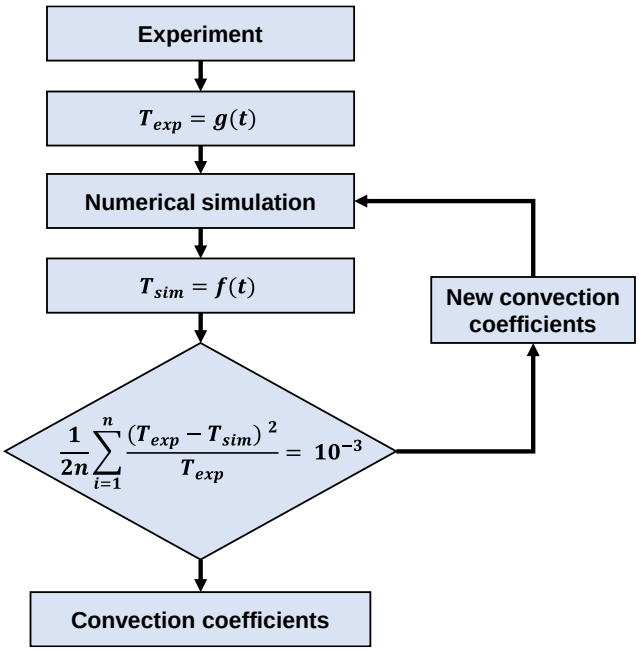

Fig.4 *Flowchart to determine the heat convection coefficients*

3.3. Heat treatment simulation

3.3.1. Thermal calculations

Assuming that the thermal and mechanical problems are uncoupled [6], the thermal equations governing the heat treatment problem can be written as:

$$\begin{cases} \nabla(\lambda \nabla \mathrm{T}) = \rho C_p \dfrac{\partial T}{\partial t} \\ \dot{Q} = -h\, A\, \Delta T \end{cases} \qquad \text{Eq.(1)}$$

where λ is the thermal conductivity, ρ is the density, C_p is the specific heat, $\dot{Q}$ is heat transfer, h is the heat transfer coefficient, A is the surface area and $\Delta T = (T_f - T_s)$ is the difference in temperature between the solid surface T_s and the surrounding fluid T_f . The needed thermophysical properties i.e. specific heat, thermal conductivity and density are temperature dependent (see **Fig.5**) and taken from the literature [6]. This data is difficult to find since they are confidential for the suppliers of the materials. However, Pechiney [6] was the only source of these thermo-dependent properties for the AA7075. The finite element method using SYSWELD© software was used to solve this problem. The calculation of the thermal gradient requires the use of small elements and time increments. The plate has been meshed with 31,920 hexahedral elements, refined on the edges (0.625 x 0.625 x 0.156 mm). The external surfaces of the simulated part were submitted to 18°C during the quenching and to 20°C during tempering.

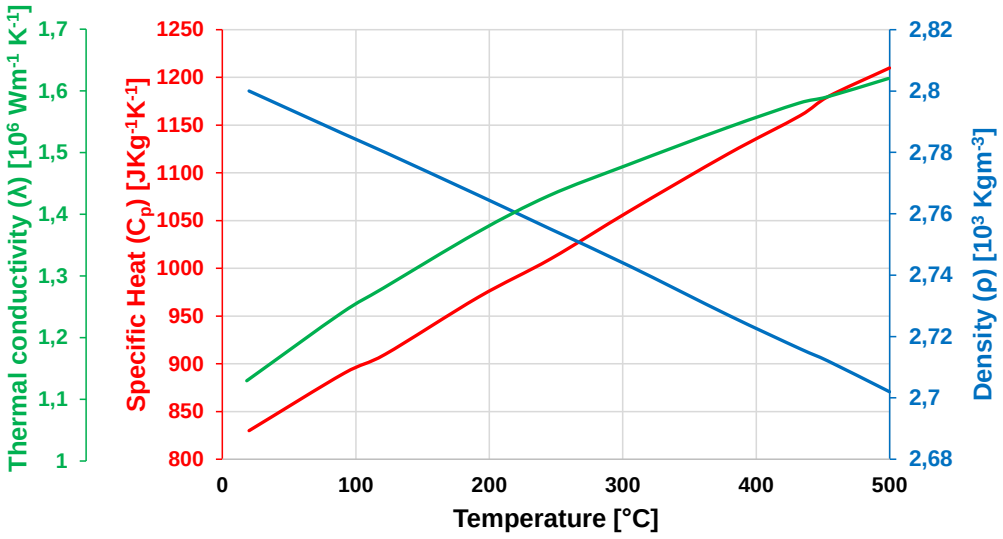

Fig.5 *Thermal conductivity, specific heat and density in function of temperature for 7075 Al alloy*

3.3.2. Mechanical calculations

During the mechanical calculations, the material is considered as isotropic and the rheological behavior of the material is non-viscous as strain rate are here quite low. Finally, the same mesh was used as in the thermal calculations. The constitutive equation is:

$$d\varepsilon_{ij}^{t} = d\varepsilon_{ij}^{e} + d\varepsilon_{ij}^{p} + \delta_{ij} d\varepsilon_{th} \qquad \text{Eq.(2)}$$

where $d\varepsilon_{ij}^{t}$ is the total strain increment, $d\varepsilon_{ij}^{e}$ the elastic strain increment related to the stress increment by the Hook's low, $d\varepsilon_{th}$ is the thermal strain increment related to the temperature increment by the thermal expansion coefficient α,i.e. $d\varepsilon_{th} = \alpha dT$ and δ_{ij} is the Kronecker's delta symbol. The evolution of the thermal expansion coefficient is shown in **Fig.6.**

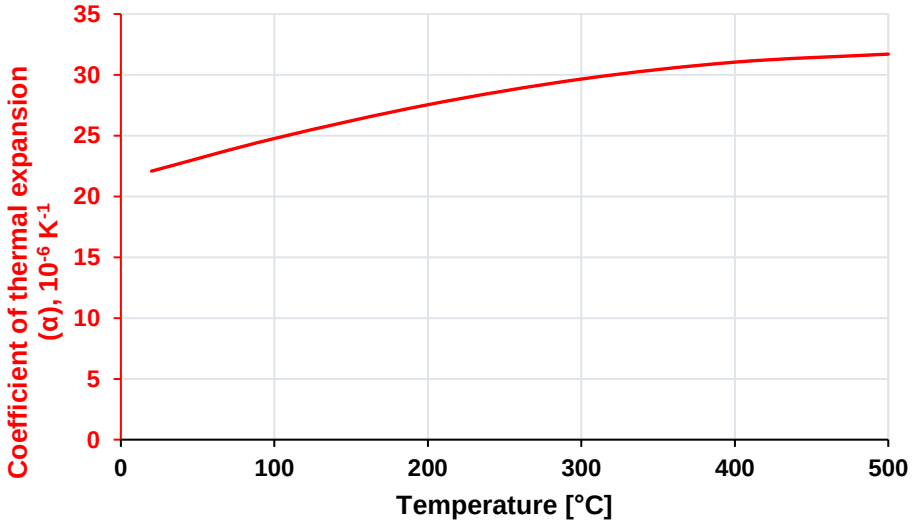

Fig.6 *Coefficient of thermal expansion in function of temperature for 7075 Al alloy*

$d\varepsilon_{ij}^{p}$ is the plastic strain increment:

$$d\varepsilon_{ij}^{p} = \frac{3}{2}\frac{d\varepsilon_{e}^{p}}{\sigma_{e}}\boldsymbol{S}_{ij} \qquad \text{Eq.(3)}$$

where σ_e is the effective stress defined as $\sigma_e = \sqrt{\frac{3}{2}\boldsymbol{S}_{ij}\boldsymbol{S}_{ij}}$, $d\varepsilon_e^p$ is the effective plastic strain defined as $d\varepsilon_e^p = \sqrt{\frac{2}{3}d\varepsilon_{ij}^p d\varepsilon_{ij}^p}$ and $\boldsymbol{S}_{ij}$ are the components of the stress deviation tensor.

Thermo-dependent isotropic hardening approximation was used to model the stress-strain curve of the material. The thermo-dependent mechanical properties are shown in **Fig.7** and **Fig.8**, taken from the literature [6**,** 27].

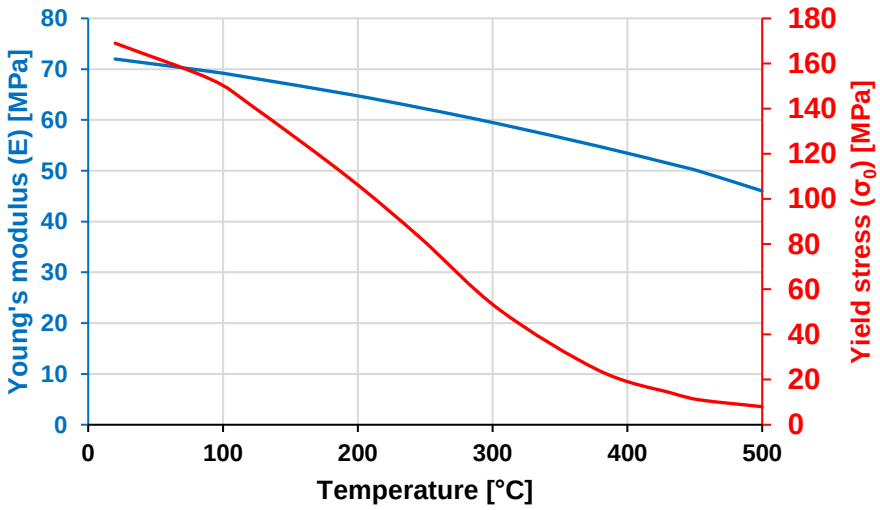

Fig.7 *Young's modulus and yield stress in function of the temperature for 7075 Al alloy*

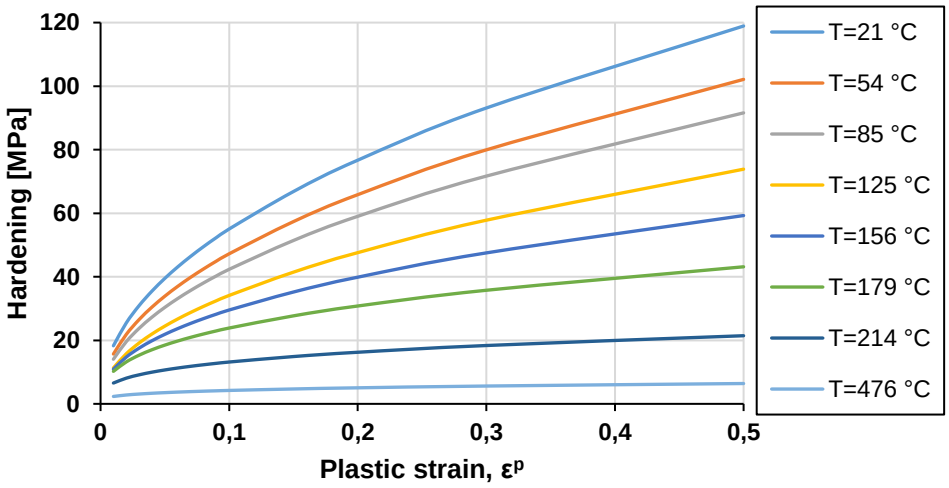

Fig.8 *Hardening curves as function of temperature of 7075 Al alloy*

The thermo-dependent mechanical properties were also taken from literature [6]. The effect of the variability of these parameters due to the heterogeneity of the material, the position of the studied part in the initial plate, the measurement errors on the residual stresses distribution will be the aim of the next publication.

4. Experimental determination of the residual stresses

4.1. Layer removal method

The layer removal method was originally introduced by Treuting and Raed [31] in 1951. It is a destructive experimental method allowing to estimate the evolution of one component of the residual stresses according of the thickness of a part. It is based on removing layers from a sample and measuring the resulting distortion. Hospers and Vogelesang [18] used this method on rolled sheet metal. Chemical etching was performed to remove the layers and then the curvature of the sheet was measured. The average stress in the removed layer can be calculated using Eq.(4) [18]. As described by Hospers and Volgelesang, after removing the layer of Δt thickness from the part, which has initially t_{i-1} thickness and r_{i-1} curvature radius, a new part thickness t_i and curvature radius r_i are obtained (see **Fig.9**). *E* is the Young modulus, ν is the Poisson ratio and σ_{YYi} is the averaged residual stress in the removed layer in Y direction [18]. The main assumption of this approach it the homogeneity of stress repartition in XY plane.

$$\sigma_{YYi} = \frac{\left(\frac{E}{12(1-\nu^2)}\right) * \left(\frac{t_i^3}{r_i} - \frac{t_{i-1}^3}{r_{i-1}}\right) - (0.5\Delta t_i \sum_{j=1}^{i-1} \sigma_{Yj} \Delta t_i)}{0.5\Delta t_i (t_i + \frac{\Delta t_i}{2})} \qquad \text{Eq.(4)}$$

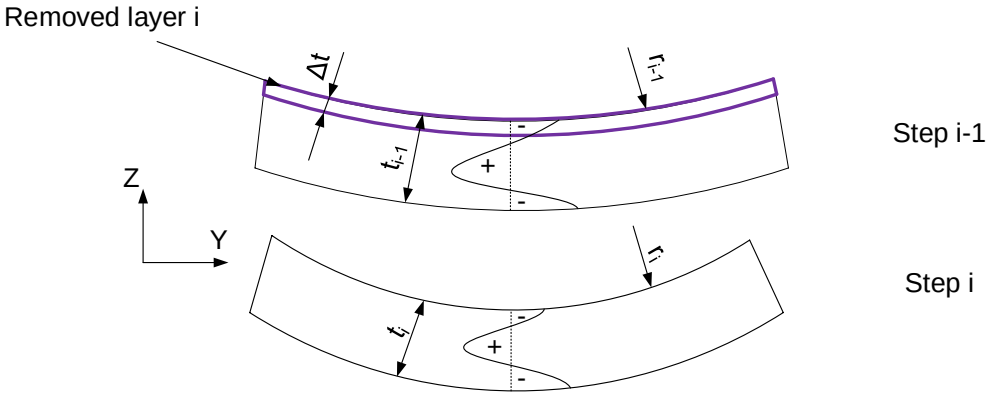

Fig.9 *Scheme of the removal layer method including the required variables*

The layers were removed by machining in two steps: machining shoulders 19 mm width and 2 mm thick before each pass, then a planing step of 61 mm width and 2 mm thick allowing removal of the entire layer as illustrated in **Fig.10.** In fact, for aluminum alloys, the layer affected by machining is of the order of 200 µm [32]. Compared to the removed layer (2 mm) and the final thickness after machining (20 mm), the effects of machining on the distortion results are negligible [24].

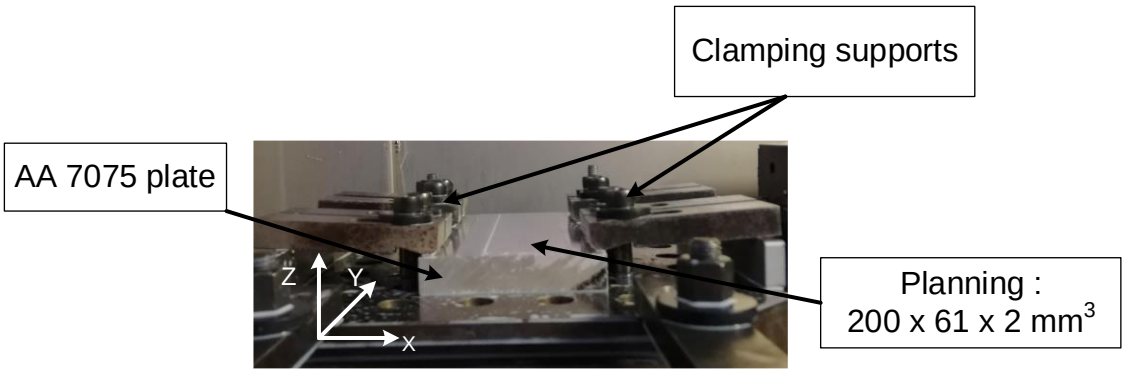

Fig.10 *Procedure for removing layers: planning operation*

Due to the assumed symmetry of the residual stress compared to the mid-plane, removing the material up to the half thickness should be sufficient [19]. Ten layers with 2 mm thickness were in consequence removed. After each step, the part was released and the midline curvature of the machined surface was measured with a Coordinate Measuring Machine (CMM).

4.2. Simulation of the removal layer method

After the simulation of the heat treatment on the aluminum plate, the removal layer method was simulated using SYSWELD© software. Bulk removal modeling was adopted to predict the distortion using an elastic model [33]. After removing the elements corresponding to the layer, the residual stresses are balanced at the level of the machined surface. A model that takes into account the distortions of the previous layers (sequence effects) and of the initial residual stresses was developed. Ten simulations (corresponding to 10 removed layers) were carried out with the same experimental methodology. First, a 2 mm thick shoulder step was made as shown in **Fig.11**. Eight clamping points modeled by a pressure in the Z direction at the contact surface of each support corresponding to a force of 20 KN was applied. Then, the planing step: which consists of the machining of a 2 mm layer and 61 mm wide and finally unclamping.

The model was built with hexahedral elements of size 5 x 5 x 0.5 mm^3 refined on the clamping zone (2.5 x 2.5 x 0.5 mm^3). During clamping, the lower surface of the part was considered to be encastred (the nodes were blocked in the three directions) with the eight clamping supports on the upper surface which ensure the maintaining in position of the part. After unclamping, and to ensure an isostatic maintenance of the part, a node N1 was blocked in the three directions X,Y and Z, a node N2 was blocked in two directions X and Z, and a node N3 was blocked in the Z direction as shown in **Fig.11**.

As two different meshes are used for heat treatment and for the removal layer method it is necessary, before the first step of material removal, to project the simulated stress field obtained from one mesh to another. To do this we use the approach proposed by Duranton et al. [34].

After each layer, the curvatures were measured on the midline plane of the simulated parts in the Y direction and subsequently the residual stresses were calculated using Eq.(4).

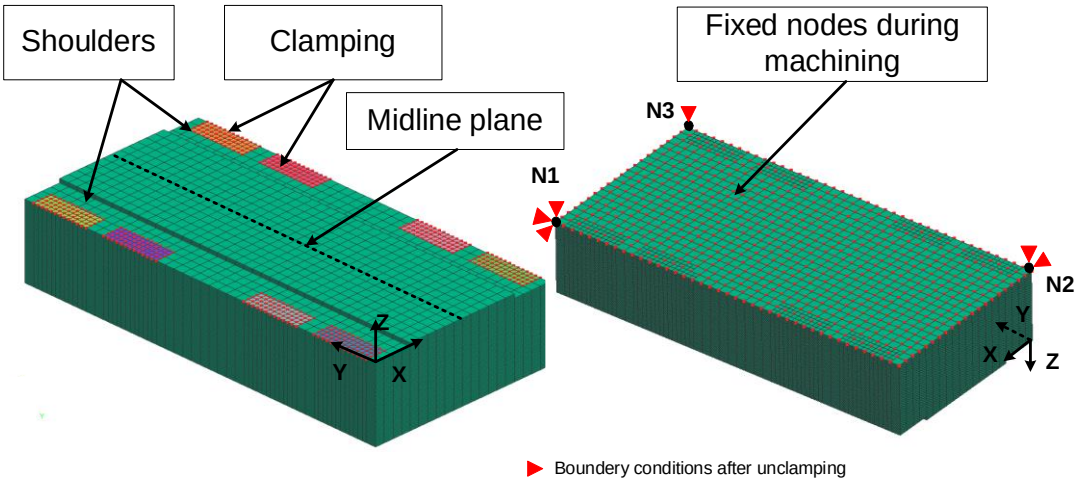

Fig.11 *Mesh and boundary conditions for the first removed layer*

A similar simulation approach will be used to reproduce material removal during machining and part deformation during the process. However, for the present approach, the material removed corresponds exactly to one or more layers of finite elements, whereas during machining the removal of material will no longer necessarily correspond to the layers of elements.

4.3. Principle of the contour method

The contour method consists of 3 steps. Step A in **Fig.12** presents the residual stresses distribution along the thickness of the plate. The sample is cut into two parts during Step B, which causes a relaxation of all the stresses present in the cut section. In step C, a linear elastic finite element analysis (FEM) is used to apply surface deflections to a numerical fit of the surface profile to recover the uncut shape. The plate was cut using wire EDM, 0.25 mm wire diameter and 0.5 mm / min cutting speed were applied [15, 35]. The cut surfaces were scanned using non-contact 3D scanner GOM, which uses a structured blue light technique.

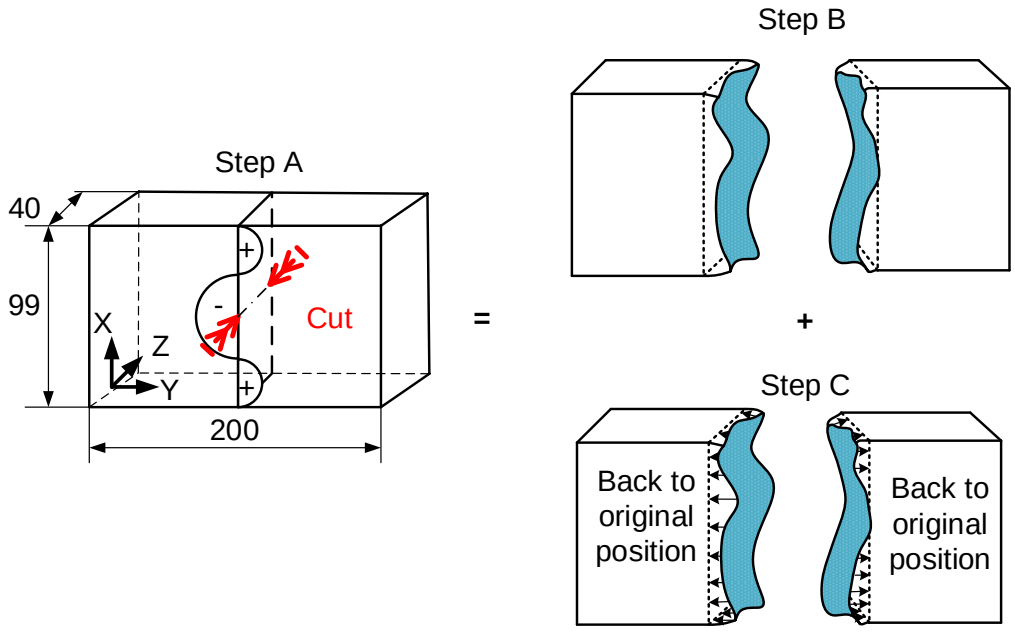

Fig. 12 *Schematic drawing illustrating the principle of the contour method for the residual stress determination across the thickness of the plate in the direction normal to the cut section.*

As shown in **Fig.13**, the step C can be decomposed in 4 sub-steps. The first sub-step of this computational framework is the alignment and averaging of the scanned surface profile data. Then, a numerical surface fitting was done using a Python script [13] to smooth the data and to impose the FEA boundary conditions (Sub-Step 2). After this, FEA preprocessing was carried out, in which an elastic calculation was performed with 8-noded quadrilaterals mesh. The boundary conditions were defined using an ABAQUS CEA script [13] (Sub-step 3). Finally, the post-processing step (Sub-step 4), in which the residual stresses results at the nodes, can be displayed.

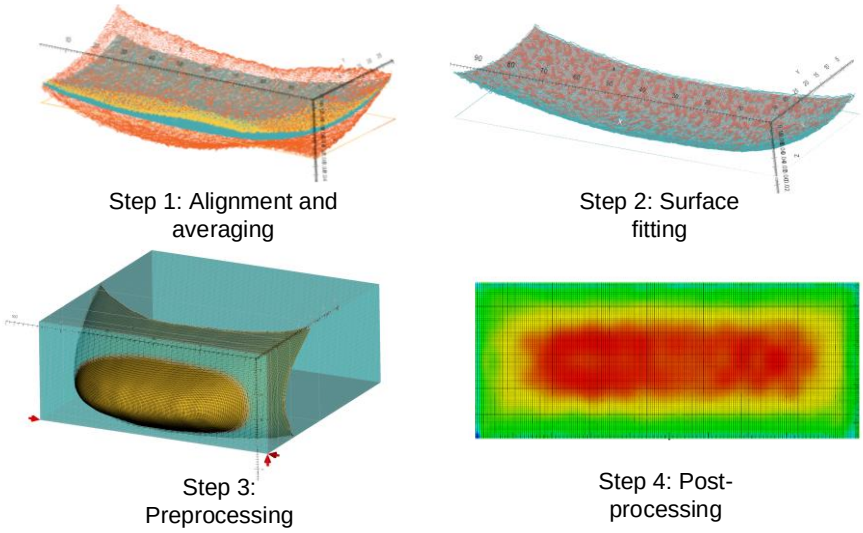

Fig.13 *Contour Method process using Python script*

5. Results and discussion

5.1. Heat treatment simulation

The results of the convection coefficient with water during quenching are shown in **Fig.14**. The curve of the heat convection coefficient in function of the temperature highlights that there are a physical phenomena of calefaction at the beginning of the quenching and then the forced convection. During this procedure, the convection coefficient increases until reaching a maximum value of h = 10 591 W.m^{-2}.K^{-1} at T = 250 °C. Then, the convection coefficient starts to decrease until it reaches a value of h = 3584 W.m^{-2}.K^{-1} at T = 41 °C. The temperature at near surface measured by the thermocouple T5 (**Fig.3**) was chosen as the reference temperature for the optimization. A strategy was adapted by dividing the entire cooling period in the water into 10 sub-periods. The goal is to optimize iteratively the sub-periods in order to determine the set of coefficients.

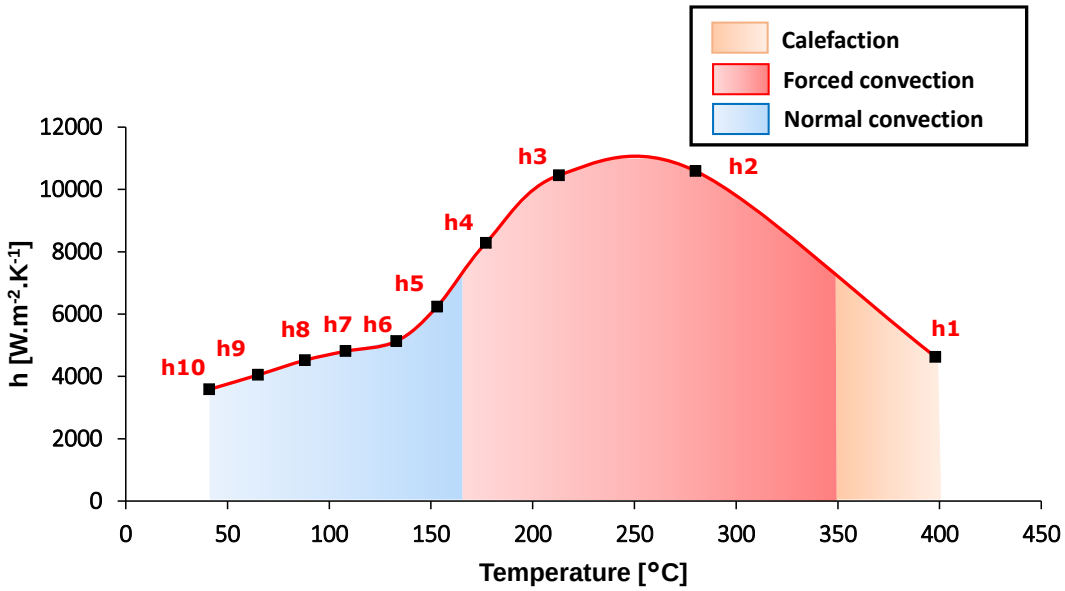

Fig.14 *Evolution of the heat convection coefficient with water as a function of the temperature*

Using these values of the heat convection coefficients in function of the temperature, a quenching simulation of AA 7075-T6 part was performed. **Fig.15** shows the simulated and measured curves of the temperature measured by the two thermocouples T1 and T5 during cooling for the ten sub-periods during the optimization.

A good agreement between experimental and simulated results is visible in **Fig.15**. The evolution of the temperature during quenching is a key point for the residual stresses generation. Therefore, the values of heat convection coefficient with water will be taken as input data for the thermomechanical simulation of the heat treatment. The experimental results show a sudden drop in temperature during the quenching process between 12 s to 13 s from the beginning of the quenching which can be explained as follows. The calefaction phenomenon is due to the vapor layer around the part, which slows down the cooling. At the temperature between 150 °C and 100 °C, this layer disappears and then the part is in direct contact with water. For this reason, cooling becomes fast until stabilization after only one second [36].

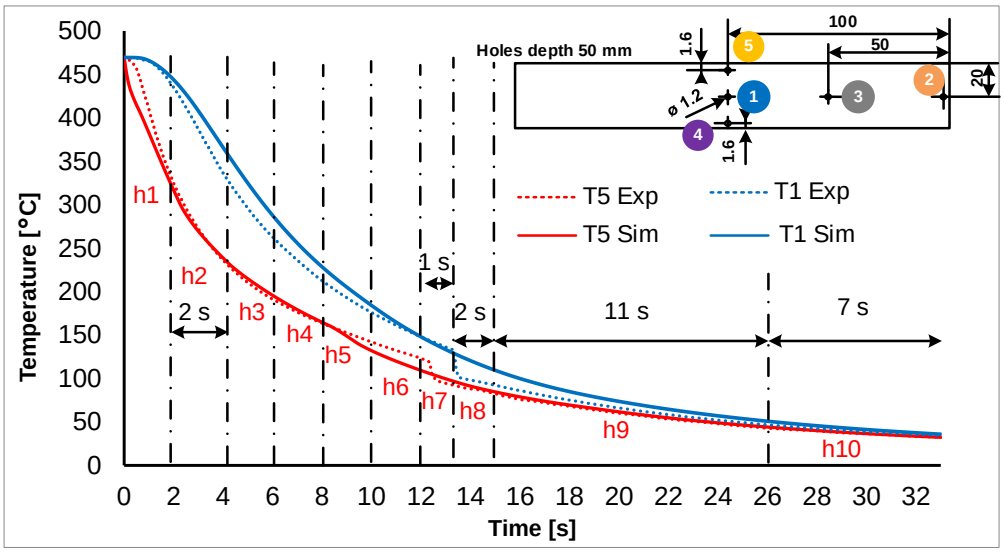

Fig.15 *Simulated and measured cooling curves (thermal convection with water)*

The same procedure was applied to determine the value of the heat convection coefficient with air during the tempering. Given the slowness of the cooling during this procedure, one coefficient of h_{air} = 6.33 W.m^{-2}.K^{-1} was obtained and used later for the heat treatment simulation.

5.2. Residual stresses results

5.2.1. Layer removal method

A comparison between the measured and simulated curvatures of the deformed parts was performed after each pass. **Fig.16** shows the midline curvature after the removal of the fifth layer. This figure proves that the machining model is capable of predicting the distortion results with an error of 9% between both curvatures. It also demonstrates that the simulated residual stresses through the heat treatment are close to those in the real part. To determine the radius of the curvature, a nonlinear curve fitting was applied. Based on these curvature values and as explained in section 3.1, the residual stresses can be calculated.

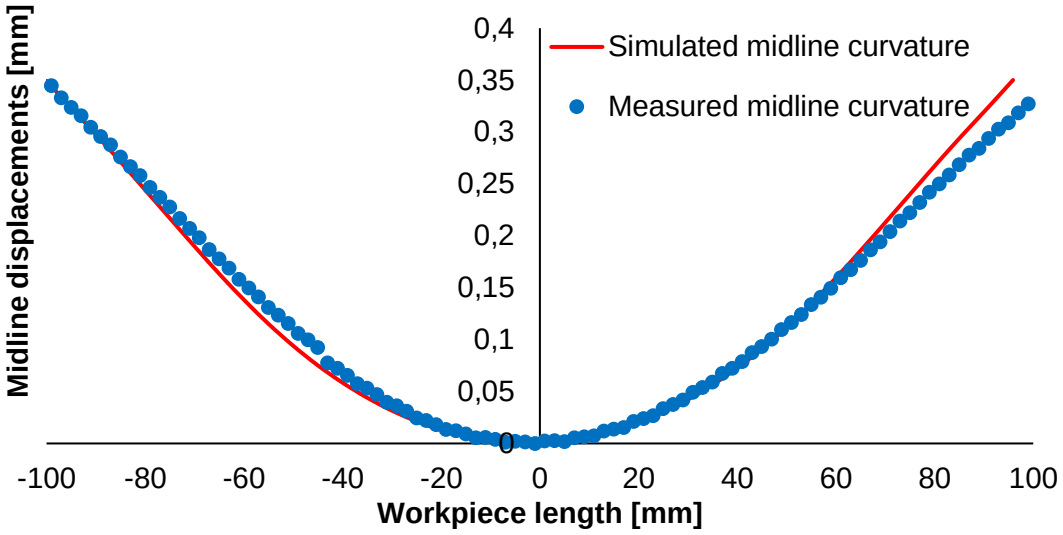

Fig.16 *Midline curvature after removing the fifth layer (1/2 of the total removed material)*

Fig.17 shows the experimental and simulated residual stresses obtained with the layer removal method. The results show the same trends for both cases. In fact, the residual stresses are compressive up to 7 mm from the surface, and then tensile until the center of the plate. At the surface, a stress of -165 ± 10 MPa was measured, while a stress of -231 MPa was simulated. For the first removed layer, the distortion is small which leads to a high value of the curvatures radii. Based on Eq.(4), the small variation of the high curvature value results in a large difference in the calculated residual stress, this explain the difference between the measured and simulated residual stresses in the first layer. Although in terms of distortion, the gap between the simulated and measured curvatures is 0.04 mm. A tensile stress of 87 MPa was also measured at the center.

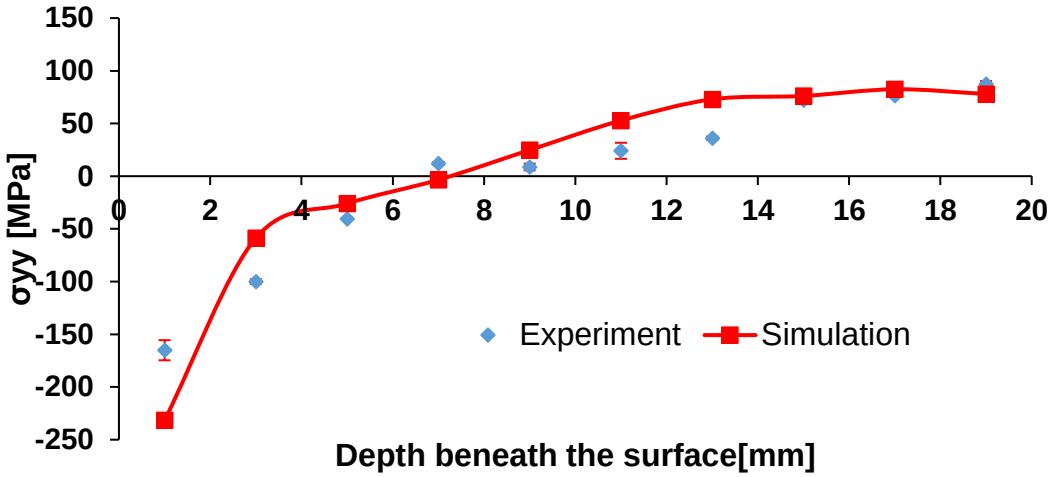

Fig.17 *Experimental and simulated residual stresses distributions in the part induced by heat treatment using layer removal method*

Based on this method, the average residual stresses of the entire removed layer can be calculated. Nevertheless, after the heat treatment, the residual stress distribution into the part is not uniform because of the temperature gradient during quenching. This phenomenon cannot be investigated using this method since it measure only the residual stresses across the depth of the part. For this reason, contour method was also performed.

5.2.2. Contour method

Using the contour method, the normal residual stress to the cut surface can be measured. During the quenching operation, thermal gradients generate strain and stresses. Actually, the quenched part can be divided into two zones: a surface zone and a core zone. At the beginning of quenching, the surface zone cools faster than the core zone. In this case, the core will prevent the deformation of the surface. The core is therefore in compression while the surface is in tension. When the core is cooled down, it will be prevented from being strained by the surface.

Fig.18 shows the residual stresses results in Y direction (σ_{YY}), obtained by the contour method and by the heat treatment simulation. **Fig.18 (a)** shows the simulated residual stresses map induced by heat treatment. This figure shows that the induced residual stress by heat treatment is not uniform. In fact, the residual stresses are compressive until 8 mm from the surface and then tensile until the center. It shows also that the induced residual stresses are symmetrical compared to the middle plane since the same thermal boundary conditions were used on all the surfaces of the simulated part. The results of the contour method show the same residual stress distribution especially the thickness of the compressive layer as shown in **Fig.18 (b)**. It validates also the symmetrical simulated residual stresses distribution.

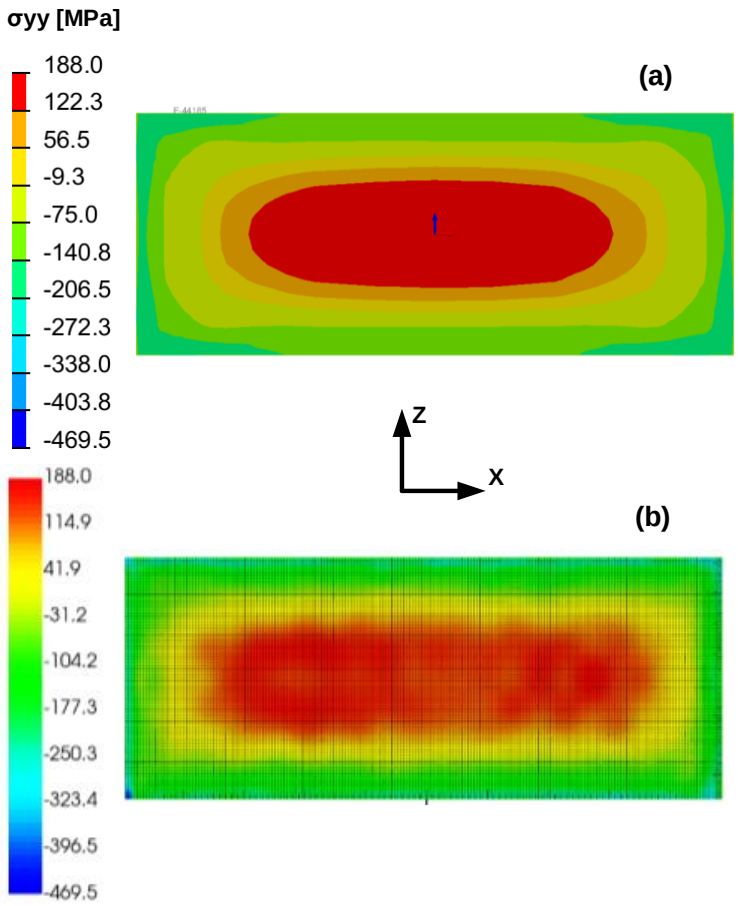

Fig.18 *Distribution of* $\boldsymbol{\sigma_{YY}}$ *residual stress in the cross section obtained by (a) numerical simulation of heat treatment; (b) contour method*

Fig.19 (a) shows that the results obtained by the contour method and those obtained by numerical simulation are nearly similar. The profile at 25 mm from the surface in X direction through the thickness of the part was investigated. Compressive stresses up to 8 mm from the surface, then tensile stresses until the center of the plate. It shows also that the residual stress profile is symmetrical compared to the middle plane. At the center of the part, a value of σ_{YY}= 182 MPa of tensile residual stresses were simulated compared to σ_{YY}= 155 MPa measured using the contour method. At the surface, about σ_{YY}= -136 MPa compressive residual stresses were simulated compared to σ_{YY}= -216 MPa measured. **Fig.19 (b)** presents the residual stress profile at the midline of the cross section through the width of the plate. It demonstrates that the heat treatment model represents well the real residual stresses distribution on the plates.

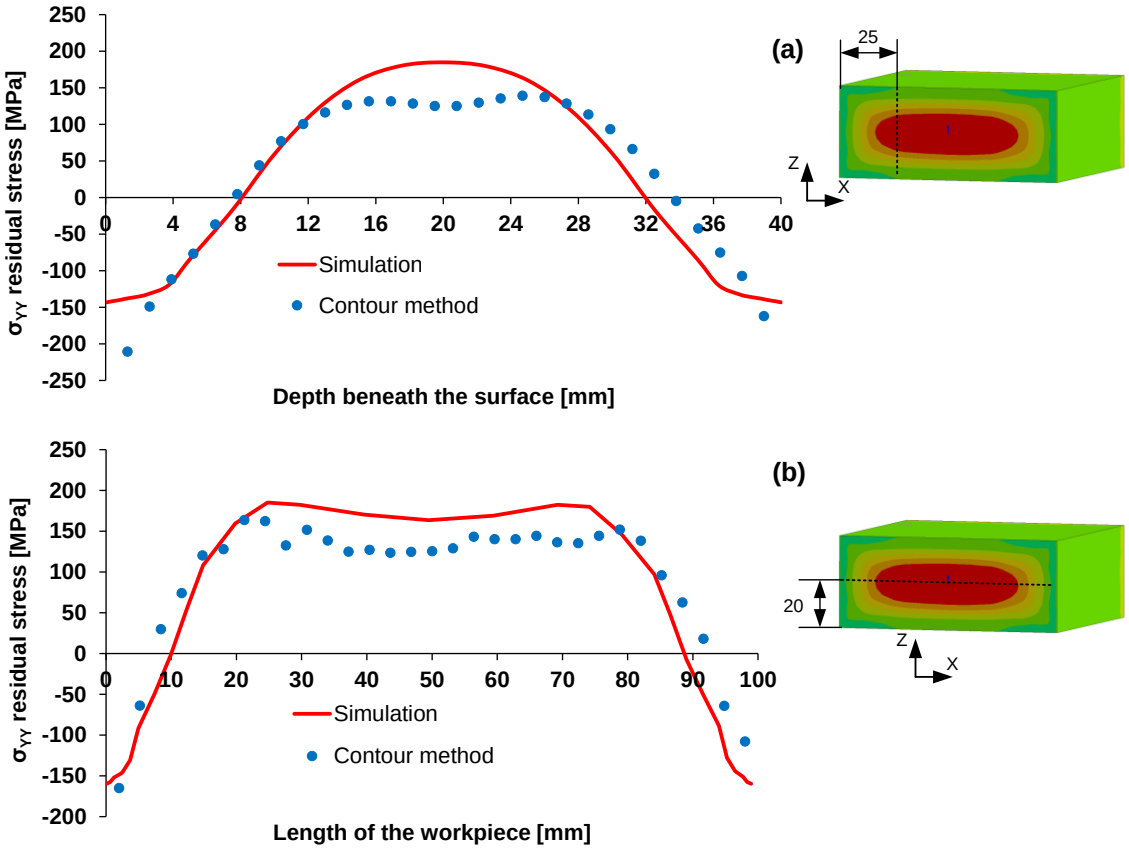

Fig.19 *Comparison of the residual stress profiles between the contour method and the simulation of heat treatment; (a) The residual stress profile* $\boldsymbol{\sigma_{YY}}$ *at 25 mm from the surface in X direction through the thickness of the part; (b) The residual stress profile* $\boldsymbol{\sigma_{YY}}$ *of the midline of the cross section through the width of the plate*

6. Conclusions

In this work, a thermomechanical model was developed to simulate the heat treatment process of the AA 7075-T6 using SYSWELD© software. To build this model, heat treatments were carried out with instrumented parts in order to determine the heat convection coefficients with water and air using the inverse method (optimization algorithm).

To validate the residual stresses distribution after the heat treatment, two methods were applied and discussed:

- The layer removal method: the experimental results were compared to the simulated results calculated from the simulation of this method. A material removal model, which takes into consideration the sequence and initial residual stresses effects, was developed. The results show that the proposed model is capable of predicting part distortions with an error of 9% compared to the measured results.
- Due to the effects of the thermal gradient, contour method was also performed and experimental residual stresses results were compared to the simulated ones induced by heat treatment. The results demonstrate that there is a good agreement between the simulated and measured RS distributions.

This work presents a guideline to simulate and validate the residual stresses distribution induced by heat treatment of AA 7075-T6 alloy. Based on this methodology, the heat treatment and material removal models were validated using experimental results.

Based on the developed model all the components of the residual stresses can be predicted. These residual stresses distribution will allow to predict distortion for more complex geometries, such as those produced by machining in the aerospace sector.

Acknowledgments

The authors would like to thank the National Research Agency for the financial support (IMaDe project ANR-19-CE10-0002) and ESI group for their support in providing SYSWELD software.

References

[1] J. Wang, « Prediction of distortion induced by machining residual stresses in thin-walled components », *Int J Adv Manuf Technol*, p. 10, 2017.

[2] S. Masoudi, S. Amini, E. Saeidi, et H. Eslami-Chalander, « Effect of machining-induced residual stress on the distortion of thin-walled parts », *Int. J. Adv. Manuf. Technol.*, vol. 76, nº 1-4, p. 597-608, 2015.

[3] X. Cerutti et K. Mocellin, « Influence of the machining sequence on the residual stress redistribution and machining quality: analysis and improvement using numerical simulations », *Int. J. Adv. Manuf. Technol.*, vol. 83, nº 1-4, p. 489-503, 2016.

[4] M. Koç, J. Culp, et T. Altan, « Prediction of residual stresses in quenched aluminum blocks and their reduction through cold working processes », *J. Mater. Process. Technol.*, vol. 174, nº 1-3, p. 342-354, 2006.

[5] M. B. Prime et M. R. Hill, « Residual stress, stress relief, and inhomogeneity in aluminum plate », *Scr. Mater.*, vol. 46, nº 1, p. 77-82, 2002.

[6] P. Jeanmart et J. Bouvaist, « Finite element calculation and measurement of thermal stresses in quenched plates of high- strength 7075 aluminium alloy », vol. 1, p. 5, 1985.

[7] N. S. Rossini, M. Dassisti, K. Y. Benyounis, et A. G. Olabi, « Methods of measuring residual stresses in components », *Mater. Des.*, vol. 35, p. 572-588, 2012.

[8] K. Moussaoui, S. Segonds, W. Rubio, et M. Mousseigne, « Studying the measurement by X-ray diffraction of residual stresses in Ti6Al4V titanium alloy », *Mater. Sci. Eng. A*, vol. 667, p. 340-348, 2016.

[9] J D.A. Tanner et J. S. Robinson « Residual Stress Prediction and Determination Aluminum Alloy Forgings in 7010 Aluminum Alloy Forgings », Exp. Mech., vol. 51, no 6, p. 981-993, 1999.

[10] I. C. Noyan, J. B. Cohen, J. B. Cohen, et J. B. Cohen, *Residual stress: measurement by diffraction and interpretation*. New York etc: Springer-Verlag, 1987.

[11] G. E. Totten, M. A. H. Howes, et T. Inoue, Éd., *Handbook of residual stress and deformation of steel*. Materials Park, Ohio: ASM International, 2002.

[12] J. S. Robinson, D. A. Tanner, C. E. Truman, et R. C. Wimpory, « Measurement and Prediction of Machining Induced Redistribution of Residual Stress in the Aluminium Alloy 7449 », Exp. Mech., vol. 51, no 6, p. 981-993, 2011.

[13] M. J. Roy, N. Stoyanov, R. J. Moat, et P. J. Withers, « pyCM: An open-source computational framework for residual stress analysis employing the Contour Method », *SoftwareX*, vol. 11, p. 100458, 2020.

[14] M. B. Prime, « Cross-Sectional Mapping of Residual Stresses by Measuring the Surface Contour After a Cut », *J. Eng. Mater. Technol.*, vol. 123, nº 2, p. 162-168, 2001.

[15] F. Hosseinzadeh, J. Kowal, et P. J. Bouchard, « Towards good practice guidelines for the contour method of residual stress measurement », *J. Eng.*, vol. 2014, nº 8, p. 453-468, 2014.

[16] F. Hosseinzadeh, P. Ledgard, et P. J. Bouchard, « Controlling the Cut in Contour Residual Stress Measurements of Electron Beam Welded Ti-6Al-4V Alloy Plates », *Exp. Mech.*, vol. 53, nº 5, p. 829-839, 2013.

[17] P. Pagliaro, M. B. Prime, H. Swenson, et B. Zuccarello, « Measuring Multiple Residual-Stress Components using the Contour Method and Multiple Cuts », *Exp. Mech.*, vol. 50, nº 2, p. 187-194, 2010.

[18] F. Hospers et L. B. Vogelesang, « Determination of residual stresses in aluminum-alloy sheet material: In method described by the authors, thin layers are removed by chemical etching, which induces an increasing curvature of the sheet. The initial distribution of the residual stress is derived from curvature measurements », *Exp. Mech.*, vol. 15, nº 3, p. 107-110, 1975.

[19] V. Richter-Trummer, D. Koch, A. Witte, J. F. dos Santos, et P. M. S. T. de Castro, « Methodology for prediction of distortion of workpieces manufactured by high speed machining based on an accurate through-the-thickness residual stress determination », *Int. J. Adv. Manuf. Technol.*, vol. 68, nº 9-12, p. 2271-2281, 2013.

[20] P. V. Grant, J. D. Lord, et P. S. Whitehead, « Measurement Good Practice Guide No. 53 - Issue 2 », p. 70, 2006.
[21] G. S. Schajer, « Advances in Hole-Drilling Residual Stress Measurements », *Exp. Mech.*, vol. 50, nº 2, p. 159-168, 2010.
[22] A. H. Mahmoudi, S. Hossain, C. E. Truman, D. J. Smith, et M. J. Pavier, « A New Procedure to Measure Near Yield Residual Stresses Using the Deep Hole Drilling Technique », *Exp. Mech.*, vol. 49, nº 4, p. 595-604, 2009.
[23] F. Hosseinzadeh, J. Kowal, et P. J. Bouchard, « Towards good practice guidelines for the contour method of residual stress measurement », p. 16, 2014.
[24] I. Cherif, D. Cotton, G. Poulachon, J. Outeiro, A. Brosse, et J. Rebelo Kornmeier, « Instrumented clamping device and numerical simulations to study machining distortion », *Int. J. Adv. Manuf. Technol.*, vol. 105, nº 7-8, p. 3093-3103, 2019.
[25] Y. Yang, M. Li, et K. R. Li, « Comparison and analysis of main effect elements of machining distortion for aluminum alloy and titanium alloy aircraft monolithic component », *Int. J. Adv. Manuf. Technol.*, vol. 70, nº 9-12, p. 1803-1811, 2014.
[26] X. Cerutti, K. Mocellin, S. Hassini, B. Blaysat, et E. Duc, « Methodology for aluminium part machining quality improvement considering mechanical properties and process conditions », *CIRP J. Manuf. Sci. Technol.*, vol. 18, p. 18-38, 2017.
[27] H. F. Bueckner, « Field singularities and related integral representations », in *Methods of analysis and solutions of crack problems*, G. C. Sih, Éd. Dordrecht: Springer Netherlands, p. 239-314, 1973.
[28] X. Cerutti, « Numerical modelling and mechanical analysis of the machining of large aeronautical parts : Machining quality improvement », Mines ParisTech, France, 2014.
[29] S. Hassini, « Qualification multi-critères des gammes d'usinage: application aux pièces de structure aéronautique en alliage Airware® », BLAISE PASCAL - Clermont II, Clermont Ferrand, 2015.
[30] A. I. H. Committee et J. Douthett, *ASM handbook: Heat treating*. ASM International, 1991.
[31] R.G.Treuting et W.T.Read, JR, « A. Mechanical determination of biaxial residual stress in sheet materials» Journal of applied physics, 1951.
[32] B. Denkena et L. D. Leon, « Milling induced residual stresses in structural parts out of forged aluminium alloys », *Int. J. Mach. Mach. Mater.*, vol. 4, nº 4, p. 335, 2008.
[33] K. Ma, R. Goetz, et S. K. Srivatsa, « Modeling of Residual Stress and Machining Distortion in Aerospace Components RS», Defense Technical Information Center, Fort Belvoir, VA, 2010.
[34] P. Duranton, J. Devaux, V. Robin, P. Gilles, et J. M. Bergheau, « 3D modelling of multipass welding of a 316L stainless steel pipe », *J. Mater. Process. Technol.*, vol. 153-154, p. 457-463, 2004.
[35] C. Liu et X. Yi, « Residual stress measurement on AA6061-T6 aluminum alloy friction stir butt welds using contour method », *Mater. Des.*, vol. 46, p. 366-371, 2013.
[36] K. Ba, J. Levesque, A. Gakwaya, et S. S. Karganroudi, « Residual stress investigation of quenched and artificially aged aluminum alloy 7175 », *Int. J. Adv. Manuf. Technol.*, vol. 116, nº 5-6, p. 1537-1553, 2021.